


Micro-CT analysis of the anatomical characteristics of the stapedial annular ligament

Aydin Mohammadi¹  · Nicholas Jufas^{1,2} · Philip Sale³ · Kirsti Lee¹ · Nirmal Patel^{1,2} · Stephen O'Leary³

Received: 20 September 2015 / Accepted: 1 February 2016 / Published online: 15 February 2016
© Japanese Association of Anatomists 2016

Abstract The oval window region has recently been identified as a potential route for drug diffusion into the inner ear. Locally applied gadolinium and trimethylphenylammonium (TMPA) have been shown to directly diffuse into the vestibule through the oval window region. Given the potential importance of the oval window region in the diffusion of substances into the inner ear, this work aimed to use micro-CT to obtain a data set of anatomical characteristics of the annular ligament of the stapes in the human temporal bone, a region thus far poorly studied. Twenty-one temporal bones were micro-dissected to preserve the otic capsule and allow perfusion of fixative stains into the inner ear. The specimens were scanned with micro-CT methods to provide 3D reconstructions and measurement. The 3D reconstructions were able to demonstrate an undisturbed stapes footplate and annular ligament from which measurements could be taken. This study found a wide variance in the volumes and thicknesses of the stapedial ligaments. There was a positive correlation between the size of the stapes footplate and the annular ligament.

Keywords Oval window · Ear · Stapes · X-ray microtomography · Vestibule · Labyrinth · Otolaryngology

Introduction

The mechanism for drug diffusion from the middle to inner ear had been widely accepted as occurring through the round window into the scala tympani with local communication to the scala vestibuli (Salt et al. 2003; Salt and Ma 2001). Recently, the oval window region has been identified as another potential route. A study (King et al. 2011) calculated through the use of high-resolution MR imaging that 90 % of the intravestibular gadolinium (Gd) that had been applied to the middle ear communicated directly into the vestibule in the region of the stapes and thus the oval window. A subsequent study (Salt et al. 2012) used uptake of trimethylphenylammonium (TMPA) to qualitatively conclude that 30–40 % entered the vestibule in the vicinity of the stapes. This research has heightened interest in the morphology of the stapes as a potential vehicle for drug delivery in the clinic. Now it appears that the size of the footplate, its thickness, and that of the surrounding annular ligament might influence the diffusion of therapeutic agents through the oval window niche (Tanaka and Motomura 1981; Zou et al. 2005, 2012). Here, we use high-resolution micro-CT imaging of the intact cadaveric temporal bone to explore morphological features of the stapes and annular ligament that might influence drug delivery via the oval window. The major and most obvious advantage of the micro-CT method is the nondestructive nature of measurements of the stapes footplate and annular ligament with both in situ.

A recent study by Sim et al. (2013) was the first use of microscopic computed tomography (micro-CT) to compare relative anatomical dimensions of human and guinea pig stapes. We extend this work by looking specifically at the stapedial annular ligament and examining the stapes footplate thickness in detail. The dimensions described herein

✉ Aydin Mohammadi
dr.aydin.mohammadi@gmail.com

¹ Deafness Research, Kolling Institute of Medical Research, Royal North Shore Hospital, Pacific Hwy, Sydney, NSW 2065, Australia

² Discipline of Surgery, Sydney Medical School, University of Sydney, Sydney, NSW, Australia

³ Department of Otolaryngology Head and Neck Surgery, University of Melbourne, Melbourne, Australia

have not been previously demonstrated in published studies and may be used to improve the modeling of drug diffusion through the stapes.

Materials and methods

Specimen preparation

Ethics approval was obtained for the use of 21 human cadaver temporal bones as low- or negligible-risk research through the Kolling Deafness Research Centre, University of Sydney. The fresh frozen bones were sourced from Science Care (Phoenix, AZ, USA) as human cadaveric tissue for nonclinical research. The extraneous soft tissue and bone external to the otic capsule were removed by microdissection. A cortical mastoidectomy was performed, followed by posterior tympanotomy. This allowed optimal visualization of the region of the stapes and vestibule. The semicircular canals were fenestrated and a cochleostomy performed at the apical turn to allow perfusion of fixative and stains into the inner ear and therefore improve visualization of the soft-tissue structures of the membranous labyrinth.

Following dissection, the specimens were preserved to prevent tissue drying and deterioration. The fixation method involved placing the specimen in phosphate-buffered Karnovsky's fixative (3 % paraformaldehyde and 0.5 % glutaraldehyde) for 5–7 days and then transferring it to a 0.1 M phosphate buffer solution (pH 7.3). After fixation, the specimens were stained en-bloc with 2 % gadolinium chloride and 2 % osmium tetroxide for 10 days. Bones were suspended in the phosphate buffer and secured within an airtight container during scanning.

Imaging

All dissected specimens were scanned with micro-CT using the Xradia MicroXCT-400 micro-computed tomography (LOT-Oriel Group, Darmstadt, Germany) unit at the University of Sydney, Australia.

3D reconstructions of DICOM data were performed using 3D-DOCTOR (Able Software Corp., Lexington, MA, USA), an advanced FDA-approved 3D modeling application. Stapes and annular ligament imaging took place in specimens with stapes in situ, thus reducing the chance of altering the data by technical error.

Scans were performed at voxel resolutions ranging from 10.5 to 16.9 μm , which was dependent on the maximal resolution achievable for the size of the specimens. Due to beam hardening from artefact as well as possible pre-scan damage to the footplate region, which was noted following CT, 12 of the 21 scans were excluded. Nine of the 21 stapes

footplates and annular ligaments were used for measurements.

The DICOM image datasets were examined by three independent researchers to ascertain suitability. The image datasets were then orthogonally sliced to allow area-of-interest measurements of the stapes footplate and annular ligament thickness, area, and volume measurements. Data entry was performed in Excel (Microsoft Corporation, Redmond, WA, USA).

Measurements

Annular ligament measurements were taken following 3D reconstructions by performing 10 point-to-point distances in the mediolateral planes at the anterior, posterior, superior, and inferior aspects of the specimens. These were then averaged for each orientation of the specimens.

Stapes footplate measurements were taken following 3D reconstruction and sectioning in the anteroposterior and superoinferior planes. Ten mediolateral point-to-point distances were taken in each plane. The mean thickness was calculated in each plane and further averaged across the three planes to ascertain the average thickness. Footplate area calculation was carried out with the area-of-interest (AOI) tool in 3D-DOCTOR by manually tracing the outside contour of the stapes footplate at its contact with the annular ligament. This was repeated three times and the mean calculated to decrease manual measurement error.

Distances were calculated in pixels, which then were converted to millimeters. This was via the calculation of voxel information provided in the DICOM files.

Results

Micro-CT generates high-resolution images of the stapes, as shown in Fig. 1. This figure visualizes the orientations in which the stapes and annular ligaments were analyzed in this study. A single left-sided stapes is presented in each of these orientations. The orientation of the stapes during measurement of the thickness of the stapes footplate is presented in Fig. 2. An example of a stapedia ligament is presented in Fig. 3.

The full set of metrics derived from the analysis is presented in Table 1; descriptive statistics are found in Table 2. These data appear to be consistent with other measurements made with micro-CT. For example, we found the stapes footplate area to be $2.82 \pm 0.49 \text{ mm}^2$, which is similar to the $2.86 \pm 0.32 \text{ mm}^2$ found by Sim et al. (2013).

Relationships between these measurements were then explored, with a view to identifying those that might be pertinent to drug delivery through the stapes. It is apparent

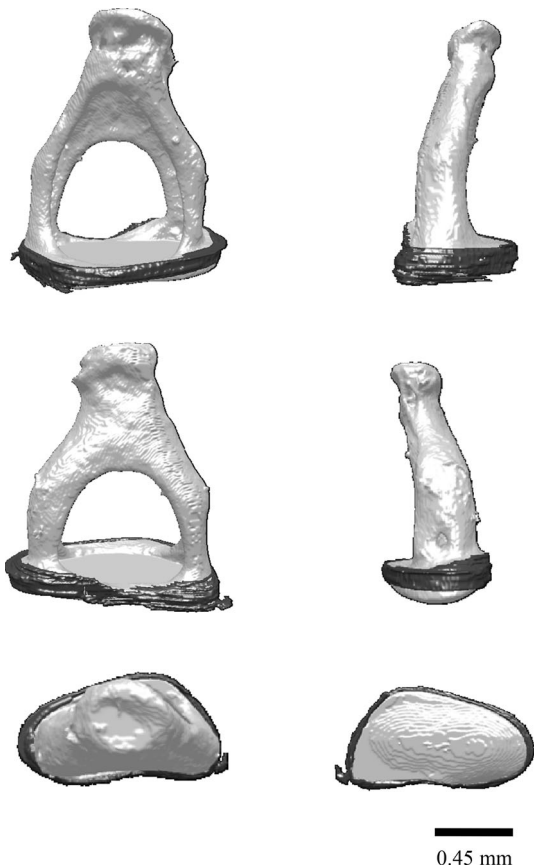


Fig. 1 3D reconstruction of one stapes and annular ligament in each of the standard orientations used in this study. *Clockwise from top left*: superoinferior, posteroanterior, anteroposterior, mediolateral, lateromedial, and inferosuperior projections

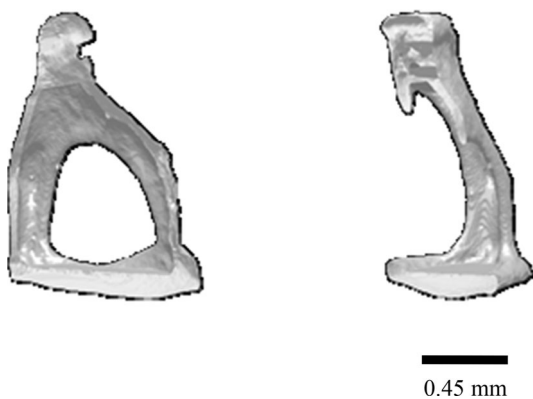


Fig. 2 Examples of cross-sections of the stapes to allow footplate measurements

that there was much greater variability in the thickness than the lateromedial distance of the stapes footplate. This suggests that the major determinant of drug diffusion might be the footplate's thickness. This is further supported by the results of a regression analysis which revealed that

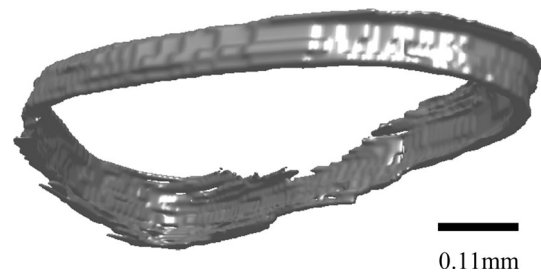


Fig. 3 Standalone reconstruction of an annular ligament

stapes volume is more strongly predicted by stapes thickness ($\beta = 0.891$, $t = 25.33$, $p < 0.0005$) than area ($\beta = 0.197$, $t = 5.80$, $p < 0.001$). It is very apparent that the annular ligament has a much lower volume than that of the stapes. The footplate has a volume that is three orders of magnitude greater than that of the annular ligament. When considering the entire data set, there were no significant correlations between metrics derived from the stapes and those derived from the annulus. However, a closer examination of the data revealed that specimen 9 had an unusual annular ligament to stapes footplate thickness ratio, so this was removed as an outlier. There was subsequently found to be strong correlations of annular thickness with stapedial thickness ($r = 0.835$, $p = 0.010$) and volume ($r = 0.077$, $p = 0.026$).

Discussion

It is apparent that there is much greater variance in the thickness than the area of the stapes footplate (when measured from the perspective of the middle ear). Although little is yet known about how drugs pass through this region, it seems likely that this may have ramifications for the diffusion of drugs through the oval window.

Thus far, the drugs that have been shown to pass into the vestibule via the oval window in experimental animals are the MRI imaging agent Gadolinium (King et al. 2011; Zou et al. 2005, 2012), the experimental drug tracer TMPA, and the aminoglycoside antibiotic gentamicin (King et al. 2013). Zou et al. (2005) presented MRI imaging supporting the entry of gadolinium into the vestibule via the stapes in the human, demonstrating that the vestibule and semicircular canals were brighter than the cochlea 2 h after intratympanic delivery. To enter directly into the vestibule, these drugs will encounter the epithelial layer of the middle ear, and beneath this the stapes footplate and annular ligament. If drug entry via the stapes is in any way analogous to that of the round window, it may be expected that permeability is limited by the epithelial layer of the middle ear. Whether either the stapes footplate or the annular

Table 1 Complete table of results

Specimen	SF area (pixels)	Mean SF thickness (mm)	Area (mm ²)	Pixel size (μ)	AL volume (Vox)	AL volume (mm ³)	AL SA (square pixels)	Mean AL thickness (mm)
81247_A2	10473	0.12935	2.284096619	14.768	42020	0.000620551	24650	0.26392
100851	18954	0.16461	2.287683175	10.9862	80073	0.000879698	49650	0.28096
110970	14478	0.17462	3.157562384	14.768	48903	0.0007222	30196	0.30529
80904_6236	10580	0.20779	2.307432658	14.768	46859	0.000692014	25067	0.47166
110922	12694	0.25674	2.768483002	14.768	80517	0.001189075	43791	0.32405
110942	15192	0.29831	3.30972912	14.768	36999	0.000546401	27503	0.30268
80938	26490	0.39475	2.92642215	10.5106	81590	0.00085756	27205	0.56983
80388	11489	0.43031	3.294901025	16.9348	60253	0.001020373	31662	0.63975
110968	13895	0.49617	3.030413684	14.768	45697	0.000674853	30946	0.27054

SF stapes footplate; mm millimeters; mm² square millimeters; μ micrometers; Vox voxels; AL annular ligament; mm³ cubic millimeters; SA surface area

Table 2 Mean footplate and annular ligament measurements

Stapes descriptive statistics					
	N	Minimum	Maximum	Mean	Std. deviation
SF_Thickness	9	0.129	0.496	0.284	0.13
SF_Area	9	2.284	3.31	2.819	0.429
SF_Volume	9	0.295	1.504	0.831	0.452
AL_Thickness	9	0.264	0.64	0.381	0.142
AL_Volume	9	0.000546	0.001189	0.0008	0.000206

Measurements given in millimeters (thickness: mm; area: mm²; volume: mm³)

ligament present a boundary to permeability is not yet understood, so the results in this paper need to be interpreted with this in mind. If permeability of the bone of the footplate is found to be important, then our results would suggest that it will be its thickness rather than its size that introduces the most variability in drug diffusion between patients. If drugs traverse the annular ligament more readily, then it is clear that the surface area of this structure is very small indeed relative to that of the stapes. Therefore, a drug would need to be very much more permeable via the annulus for this to impact upon drug entry via the oval window.

A thorough understanding of drug diffusion across the middle ear into the inner ear has significant therapeutic implications. A number of clinical conditions, such as sudden sensorineural hearing loss (SSNHL), endolymphatic hydrops, and labyrinthitis can be treated by methods which involve targeting the inner ear via direct drug diffusion (Stachler et al. 2012; Syed et al. 2015). From the discussion above, it is apparent that factors other than the anatomical features studied here, such as the health of the middle ear mucosa, will likely impact upon the permeability of the drug in specific pathological situations.

It is as yet too early to know whether there will be a clinical advantage in imaging the stapes prior to drug delivery that is targeted to the oval window, but this is increasingly possible from a technical perspective. High-resolution CT (HRCT) looking directly at the morphology of the footplate region may provide information on the area of the stapes footplate, but it would struggle to provide an estimate of footplate thickness. Newer modalities such as cone beam computed tomography (CBCT) have higher resolution and may do better (Peltonen et al. 2007). But, as yet, there is no published research where CBCT has been used to make quantitative measurements looking at the middle ear structures.

Acknowledgments The study was performed without any financial grants. The authors do not have any industrial links and/or affiliations.

Compliance with ethical standard

Conflicts of interest The authors have no potential or actual conflicts of interest related to the research within this paper to declare.

References

- King EB, Salt AN, Eastwood HT, O'Leary SJ (2011) Direct entry of gadolinium into the vestibule following intratympanic applications in guinea pigs and the influence of cochlear implantation. *J Assoc Res Otolaryngol* 12:741–751. doi:10.1007/s10162-011-0280-5
- King EB, Salt AN, Kel GE, Eastwood HT, O'Leary SJ (2013) Gentamicin administration on the stapes footplate causes greater hearing loss and vestibulotoxicity than round window administration in guinea pigs. *Hear Res* 304:159–166. doi:10.1016/j.heares.2013.07.013
- Peltonen LI, Aarnisalo AA, Kortensniemi MK, Suomalainen A, Jero J, Robinson S (2007) Limited cone-beam computed tomography imaging of the middle ear: a comparison with multislice helical computed tomography. *Acta Radiol Stockh Swed* 1987(48):207–212. doi:10.1080/02841850601080465

- Salt AN, Ma Y (2001) Quantification of solute entry into cochlear perilymph through the round window membrane. *Hear Res* 154:88–97. doi:[10.1016/s0378-5955\(01\)00223-4](https://doi.org/10.1016/s0378-5955(01)00223-4)
- Salt AN, Kellner C, Hale S (2003) Contamination of perilymph sampled from the basal cochlear turn with cerebrospinal fluid. *Hear Res* 182:24–33. doi:[10.1016/s0378-5955\(03\)00137-0](https://doi.org/10.1016/s0378-5955(03)00137-0)
- Salt AN, King EB, Hartsock JJ, Gill RM, O’Leary SJ (2012) Marker entry into vestibular perilymph via the stapes following applications to the round window niche of guinea pigs. *Hear Res* 283:14–23. doi:[10.1016/j.heares.2011.11.012](https://doi.org/10.1016/j.heares.2011.11.012)
- Sim JH, Rööslö C, Chatzimichalis M, Eiber A, Huber AM (2013) Characterization of stapes anatomy: investigation of human and guinea pig. *J Assoc Res Otolaryngol* 14:159–173. doi:[10.1007/s10162-012-0369-5](https://doi.org/10.1007/s10162-012-0369-5)
- Stachler RJ, Chandrasekhar SS, Archer SM, Rosenfeld RM, Schwartz SR, Barrs DM, Brown SR, Fife TD, Ford P, Ganiats TG, Hollingsworth DB, Lewandowski CA, Montano JJ, Saunders JE, Tucci DL, Valente M, Warren BE, Yaremchuk KL, Robertson PJ, American Academy of Otolaryngology—Head and Neck Surgery (2012) Clinical practice guideline: sudden hearing loss. *Otolaryngol Head Neck Surg Off J Am Acad Otolaryngol Head Neck Surg* 146:S1–S35. doi:[10.1177/0194599812436449](https://doi.org/10.1177/0194599812436449)
- Syed MI, Ilan O, Nassar J, Rutka JA (2015) Intratympanic therapy in Meniere’s syndrome or disease: up to date evidence for clinical practise. *Clin Otolaryngol* 40(6):682–690. doi:[10.1111/coa.12449](https://doi.org/10.1111/coa.12449)
- Tanaka K, Motomura S (1981) Permeability of the labyrinthine windows in guinea pigs. *Arch Otorhinolaryngol* 233:67–75. doi:[10.1007/bf00464276](https://doi.org/10.1007/bf00464276)
- Zou J, Pyykkö I, Bjelke B, Dastidar P, Toppila E (2005) Communication between the perilymphatic scalae and spiral ligament visualized by in vivo MRI. *Audiol Neurotol* 10:145–152. doi:[10.1159/000084024](https://doi.org/10.1159/000084024)
- Zou J, Poe D, Ramadan UA, Pyykkö I (2012) Oval window transport of Gd-DOTA from rat middle ear to vestibulum and scala vestibuli visualized by in vivo magnetic resonance imaging. *Ann Otol Rhinol Laryngol* 121:119–128. doi:[10.1177/000348941212100209](https://doi.org/10.1177/000348941212100209)